Inorganic Chemistry

Article

pubs.acs.org/IC

Thorium and Uranium Carbide Cluster Cations in the Gas Phase: Similarities and Differences between Thorium and Uranium

Cláudia C. L. Pereira,[†,‡] Rémi Maurice,[§,⊥] Ana F. Lucena,[†] Shuxian Hu,[⊥] António P. Gonçalves,[†] Joaquim Marçalo,*[,†] John K. Gibson,[∥] Lester Andrews,[¶] and Laura Gagliardi*[,⊥]

[†]Unidade de Ciências Químicas e Radiofarmacêuticas, IST/ITN, Instituto Superior Técnico, Universidade Técnica de Lisboa, 2686-953 Sacavém, Portugal

[⊥]Department of Chemistry, Supercomputing Institute and Chemical Theory Center, University of Minnesota, Minneapolis, Minnesota 55455-0431, United States

[∥]Chemical Sciences Division, Lawrence Berkeley National Laboratory, Berkeley, California 94720, United States

[¶]Department of Chemistry, University of Virginia, Charlottesville, Virginia 22904-4319, United States

Supporting Information

ABSTRACT: Laser ionization of AnC_4 alloys (An = Th, U) yielded gas-phase molecular thorium and uranium carbide cluster cations of composition $An_mC_n^+$, with $m = 1$, $n = 2-14$, and $m = 2$, $n = 3-18$, as detected by Fourier transform ion-cyclotron-resonance mass spectrometry. In the case of thorium, $Th_mC_n^+$ cluster ions with $m = 3-13$ and $n = 5-30$ were also produced, with an intriguing high intensity of $Th_{13}C_n^+$ cations. The AnC_{13}^+ ions also exhibited an unexpectedly high abundance, in contrast to the gradual decrease in the intensity of other AnC_n^+ ions with increasing values of n. High abundances of AnC_2^+ and AnC_4^+ ions are consistent with enhanced stability due to strong metal−C_2 bonds. Among the most abundant bimetallic ions was $Th_2C_3^+$ for thorium; in contrast, $U_2C_4^+$ was the most intense bimetallic for uranium, with essentially no $U_2C_3^+$ appearing. Density functional theory computations were performed to illuminate this distinction between thorium and uranium. The computational results revealed structural and energetic disparities for the $An_2C_3^+$ and $An_2C_4^+$ cluster ions, which elucidate the observed differing abundances of the bimetallic carbide ions. Particularly noteworthy is that the Th atoms are essentially equivalent in $Th_2C_3^+$, whereas there is a large asymmetry between the U atoms in $U_2C_3^+$.

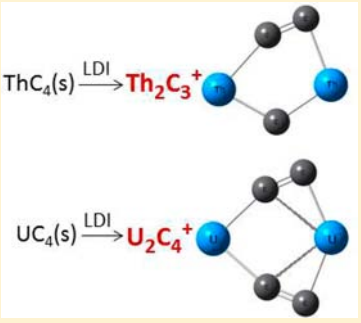

INTRODUCTION

Actinide carbides were considered efficient nuclear fuel components in the 1950s, with the potential for their use in fast reactors. Since then, there has been general disinterest in these materials because of a preference for mixed uranium−plutonium oxides as nuclear fuels. However, there is now a renewed interest in the carbide systems because of the need for new fuel types to be used in generation IV reactors.

Molecular actinide carbides provide a basis for understanding the underlying chemistry of carbide systems. Molecular AnC_n (An = Th, U; $n = 1-6$) were initially identified in Knudsen effusion mass spectrometric investigations of the metal carbides.[1−8] The formation of thorium and uranium carbide ions, AnC_n^+, $n = 1-6$, was observed in mass spectrometry studies involving plasma and thermal ionization sources.[9,10]

Recently, laser evaporation of carbon-rich uranium/carbon alloys followed by atom reactions in argon led to the formation of UC and UC_2, identified by matrix-isolation IR spectroscopy and quantum-chemical calculations.[11,12] The linear structure of UC_2 (CUC) was apparently preferred as a result of the consecutive reactions of atomized U and C, U + C → UC and UC + C → CUC; evidence was also found for bicyclic $U(CC)_2$ and tricyclic $U(CC)_3$ species.[11,12] Recent theoretical calculations for molecular UC_2 also indicated that the linear arrangement is higher in energy in comparison with that for triangular structures.[13,14] A symmetric triangular structure was computed for ThC_2,[13] improving previous calculations that had found an asymmetric L-type structure.[15] This computational study of thorium carbides also indicated that ThC_4 has a planar fan-type structure.[15] Symmetrical triangular structures have also been computed for the ground states of PuC_2 and AmC_2.[16] A theoretical study of the first-row transition-metal dicarbide cations MC_2^+ (M = Sc−Zn) has pointed to a preference for a C_{2v}-symmetric arrangement over the linear geometry, in particular for early transition metals.[17]

Laser desorption/ionization (LDI) or laser ablation (LA) coupled to mass spectrometry, sometimes comprising a cluster source, has produced many novel cluster species.[18−21] In the case of metal−carbon clusters, the metallocarbohedranes and metallofullerenes are of special note.[21−23] Smalley and co-workers used a laser vaporization cluster source and a UO_2−graphite composite system to produce a series of $U@C_n$ species and unveil the stabilization of C_{28} as $U@C_{28}$.[24] Evidence for the

Received: April 28, 2013
Published: September 18, 2013

   dx.doi.org/10.1021/ic401058b | Inorg. Chem. 2013, 52, 10968−10975

formation of $U_2@C_n$, beginning with $U_2@C_{50}$, was also presented.[24] A computational study has revealed that U_2 does not fit in the C_{60} cavity, and in a larger cavity, like C_{70} or C_{84}, U_2 preferentially binds the internal walls of the cavity and the U−U bond no longer exists.[25] Very recently, Marshall, Kroto, and co-workers also used a cluster source to reexamine the formation of $U@C_{28}$ as a dominant species and precursor for larger $U@C_n$ structures.[26]

Several metal carbide cluster cations have been generated by LDI/LA directly coupled to Fourier transform ion-cyclotron-resonance mass spectrometry (FTICR/MS).[27−32] This type of experimental setup was previously used by us to produce cationic and anionic uranium oxide clusters in the gas phase.[33] Here we report that LDI/LA of AnC_4 alloys (An = Th, U) readily yields gas-phase thorium and uranium carbide cluster cations, with unanticipated preferences for some compositions. To determine the origin of the disparities observed for the $An_2C_3^+$ and $An_2C_4^+$ clusters (with the former being particularly abundant for thorium and nearly absent for uranium and the latter being the most abundant bimetallic species for uranium), density functional theory (DFT) calculations were performed to determine the intrinsic stabilities of the corresponding species.

EXPERIMENTAL DETAILS

The experiments were performed in an Extrel/Finnigan FTMS 2001-DT FTICR/MS instrument, with a 3 T magnet and an "internal" source design in which the sample sits close to the ICR cell. A Spectra-Physics GCR-11 Nd:YAG laser (1064 nm) with an average focused power density of ca. 200 MW cm^{-2}, a pulse width of 9 ns, and a ca. 100 μm spot was used. Multiple laser pulses on the same or on fresh spots were used and yielded similar results. The potential of the front trap plate was set to 0 V for 100 μs immediately after the laser pulse. A trapping voltage of 1 V was used in all experiments. Similar results were obtained with operating pressures of $(2-5) \times 10^{-8}$ Torr of background gases (water and air) or ca. 10^{-6} Torr of argon.

For sample preparation, a standard arc-furnace melting method[34] was employed for the direct melting of cleaned thorium pellets or uranium turnings with graphite pieces under a titanium-gettered high-purity argon atmosphere. An/C mole ratios of ∼1:4 were used to form the AnC_4 alloys. An excess (ca. 20%) of graphite was used to compensate for carbon evaporation to the walls of the furnace during the synthesis; evaporation of the metals was negligible. Powder X-ray diffraction showed that the samples were mixtures of AnC_2 and graphite [see Figure S1 in the Supporting Information (SI) for an example in the case of UC_4]. The elemental compositions of the samples were determined to be $AnC_{4.0\pm0.1}$ by weight. The samples were moderately stable in air, with visible surface oxidation appearing after some days; therefore, between experiments, the samples were stored in a pure nitrogen-filled glovebox. Experiments were also performed with pressed pellets containing combinations of ThO_2 and UO_3 with an excess of powdered graphite.

Coherent ion cyclotron motion was excited by frequency-sweep irradiation over the desired bandwidth (typically from 2 kHz to 1 MHz) at a sweep rate of 2 kHz/μs. Direct-mode detection was performed over the same bandwidth, generating either 32K or 64K time domain data points before discrete Fourier transformation. Mass-resolving powers between ca. 5000 at m/z 300 and ca. 300 at m/z 3000 were typically achieved. The average mass accuracy for the range m/z 200−1000 was 5 ppm using internal calibration with known An^+, AnO^+, $AnOH^+$, ThO_2H^+, and UO_2^+ peaks; this allowed for unambiguous identification of the AnC_n^+ and $An_2C_n^+$ ions. For a larger range, e.g., m/z 500−3500, the average mass accuracy was 40 ppm, making assignment of the compositions of the thorium clusters with three or more metal atoms somewhat less definitive.

Isolation of the ions was achieved using single-frequency, frequency-sweep, or SWIFT excitation. Fragmentation of isolated product ions was studied by collision-induced dissociation (CID), in which a specific ion was excited on-resonance by a radio-frequency (rf) pulse and collided with argon present at pressures of 5×10^{-7}−1×10^{-6} Torr. Collision energies (laboratory frame) of 5−30 eV were applied in a presumed multiple-collision environment. AnC_2^+ and AnC_4^+ were reacted with oxygen, introduced into the mass spectrometer through a leak valve to pressures in the range of 5×10^{-8}−5×10^{-7} Torr. The reagent was a commercial product and was used as supplied, with >99.9% purity confirmed from electron ionization mass spectra. Rate constants, k, were determined from the pseudo-first-order decay of the relative signals of the reactant ions as a function of time at constant neutral pressures. Reaction efficiencies, k/k_{COL}, were obtained using the collisional rate constants, k_{COL}, from the theory of Su and Chesnavich,[35] calculated using the experimental molecular polarizability of the neutral reagent.[36] The neutral pressures were measured with a Bayard-Alpert-type ionization gauge calibrated using standard reactions and corrected for the relative sensitivities of the gases.

COMPUTATIONAL DETAILS

DFT-based calculations were performed using the *TURBOMOLE* program package.[37] All-electron Ahlrichs-type def-TZVP basis sets were used for the C atoms,[38] while the Th and U atoms were described with quasi-relativistic pseudopotentials with 60-electron cores.[39] First, the geometries of various spin states were optimized using different starting coordination modes, with the Perdew−Burke−Ernzerhof (PBE) functional.[40] Then the geometries of the potentially most stables structures were further optimized with the PBE0 functional,[41] and the ground-state geometries of $Th_2C_3^+$, $Th_2C_4^+$, $U_2C_3^+$, and $U_2C_4^+$ were then obtained with both the PBE and PBE0 functionals. Frequencies were computed within the harmonic approximation. The energies of the ground states of the free Th, U, and C atoms, as well as the free Th^+ and U^+ ions, were computed to obtain the complete atomization energies, as a measure of the stability of the clusters. The total energies of the monoatomic and molecular species (including the zero-point-energy correction) are reported in the SI. Note that reasonable geometries and frequencies are usually obtained with hybrid functionals for actinide carbides[11] and oxides.[42]

Electron localization function (ELF)[45,43] population analyses were performed using the *DGrid* program, version 4.6.[44] The ELF topology allows the determination of basins of chemical interest, core basins, labeled C(X), nonbonding valence basins (corresponding to lone-pair regions), labeled V(X), and bonding basins (corresponding to covalent interactions), labeled V(X,X′), allowing characterization of the nature of the chemical bonds.[46] By integrating the electron density over these basins, one can get the electron population corresponding to these basins; i.e., it is possible to know how many electrons are involved in each core region, each nonbonding region, and each covalent bond. Similarly, the electron density topology can also give information on the electronic structure of the system of interest.[47] By obtaining the average number of electrons per atom, one can get information on the effective charges of each atom. If an electron density basin is shared between two atoms, it indicates covalent bonding between these atoms, and thus care should be taken in the interpretation of the electron density population analysis.

RESULTS AND DISCUSSION

Experimentally Observed Actinide Carbide Cluster Cations. LDI/LA of AnC_4 alloys resulted in several families of thorium and uranium carbide cations with compositions $An_mC_n^+$, with $m = 1$, $n = 2$−14, and $m = 2$, $n = 3$−18, for both thorum and uranium, and $Th_mC_n^+$, with $m = 3$−13 and $n = 5$−30. Figures 1 and 2 display representative mass spectra obtained from ThC_4 samples, and Figure 3 shows a representative mass spectrum obtained from a UC_4 sample. The Th^+ and ThO^+ ions and the U^+, UO^+, and UO_2^+ ions were ejected from the FTICR cell prior to detection to enhance the signal of the less abundant thorium and uranium carbide ions. The ejections, performed by SWIFT excitation, did not affect

dx.doi.org/10.1021/ic401058b | Inorg. Chem. 2013, 52, 10968−10975

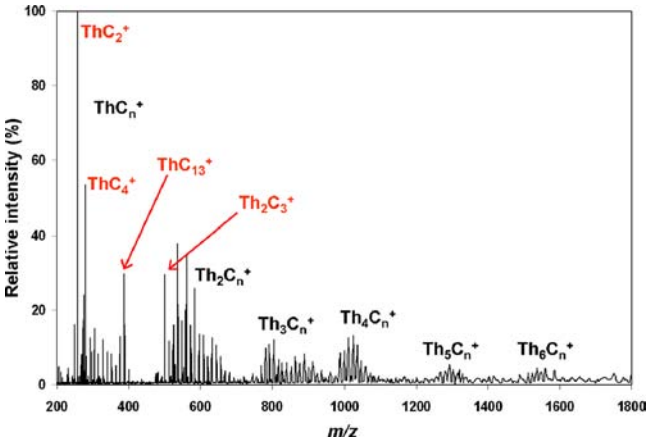

Figure 1. LDI/LA(+) mass spectrum of a ThC_4 sample (ThC_n^+–$Th_6C_n^+$ region).

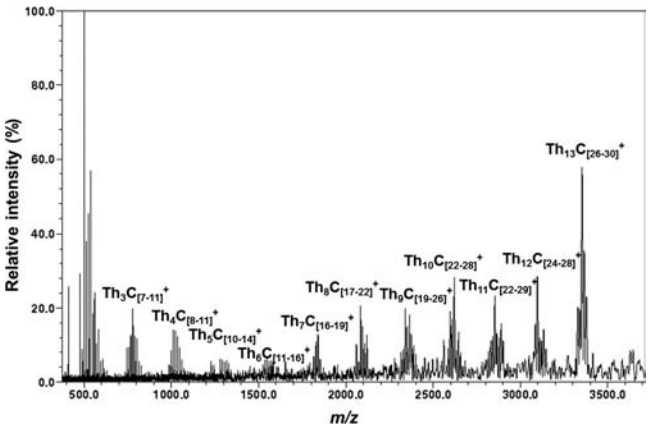

Figure 2. LDI/LA(+) mass spectrum of a ThC_4 sample ($Th_2C_n^+$–$Th_{13}C_n^+$ region).

the relative abundances of the carbide ions, as can be seen in mass spectra obtained without ejections (see Figures S2 and S3 in the SI). The attained mass-resolving powers and average mass accuracies for the range m/z 200−1000 allowed for unambiguous identification of the AnC_n^+ and $An_2C_n^+$ ions, which are the focus of this study. The mass spectral data were also clear in showing that only singly charged metal carbide species were obtained. Figure S2 in the SI shows, as an example, the ThC_{11-13}^+ region of a LDI/LA(+) mass spectrum of ThC_4, revealing ^{13}C isotopic peaks with expected relative intensities; the $^{12}C/^{13}C$ isotopomers are separated by m/z 1, indicating a charge of 1+. Tables S1−S4 in the SI present the experimental peak lists for the AnC_n^+ and $An_2C_n^+$ regions of the mass spectra of Figures 1 and 3, as well as the calculated m/z and identification of the corresponding ions.

The formation of oxycarbides in the LDI/LA process was possible as some surface oxidation of the AnC_4 samples occurred, although our synthesis method assures a negligible presence of oxygen in the products (see the Experimental Details section). It is known, for example, that in the case of titanium carbides, traces of oxygen may lead to oxycarbides.[48] In freshly prepared samples, the presence of the typical thorium and uranium oxide ions was minimal, as can be seen in Figure S3 in the SI for the case of uranium. As shown in Tables S1−S4 in the SI, a few oxygen-containing ions could be identified, but they were minor compared to the array of carbide ions formed. The mass accuracy was sufficient to distinguish ions containing nearly isobaric $^{12}C_4$ (48.0000 u) and $^{16}O_3$ (47.9847 u) in the range of focus of AnC_n^+ and $An_2C_n^+$ ions. Apparently, the excess of carbon in the samples minimizes the presence of oxygen-containing species, possibly by the formation of CO_2 during the laser ionization process.

The mechanism of formation of the thorium and uranium carbide ions by LDI/LA is uncertain, as it is with other inorganic solids, as discussed in detail by Aubriet, Muller, and co-workers.[49−51] Ions may be produced in the laser plume by gas-phase interactions of the particles formed after laser desorption/ablation (neutrals and ions, atomic and molecular species, aggregates, electrons). Cluster-ion formation may be based on the growth of smaller species by the sequential addition of neutral molecules to precursor ions. Dissociative processes may follow because of excess internal energy and collisions with neutrals in the dense laser plume. Other possible processes involve ionization of neutral clusters ablated from the

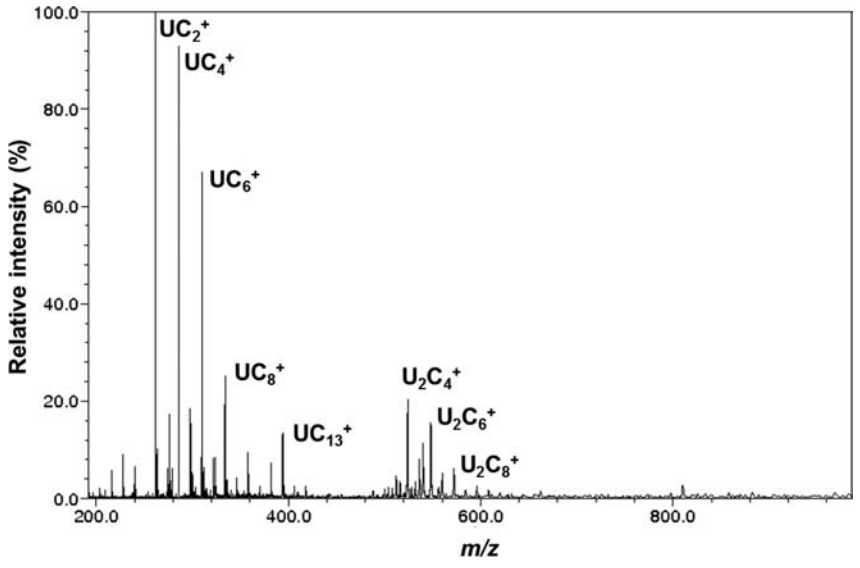

Figure 3. LDI/LA(+) mass spectrum of a UC_4 sample.

dx.doi.org/10.1021/ic401058b | Inorg. Chem. 2013, 52, 10968−10975

sample by electrons emitted from the sample surface via thermo- or photoelectronic effects.

In the present experiments, the observed thorium and uranium carbide ions most probably resulted from processes occurring in the laser plume, e.g., cationization or electron ionization of stable neutral molecular C_n and AnC_n species (such as those observed in Knudsen effusion mass spectrometric investigations of thorium and uranium carbides[1−8]). Our observation that LDI/LA of mixtures of ThO_2 or UO_3 and graphite also yielded carbide species, mainly AnC_n^+, although less efficiently and with lower abundances compared with metal and metal oxide ions, seems to indicate that the processes occurring in the laser plume are most relevant. Characterization of the AnC_4 samples as mixtures of AnC_2 and graphite (see the Experimental Details section) does not contradict these statements because it can be envisioned that, e.g., AnC_2^+ ions directly generated by laser ionization can interact with neutral C_n and AnC_n species to form AnC_n^+ and $An_mC_n^+$ ions, respectively. The presence of graphite phases in the AnC_4 samples may explain the observation of carbon clusters in the mass spectra (see Tables S1 and S3 in the SI).

The direct LDI/LA method employed in our experiments is intrinsically different from the cluster sources used to produce many different types of cluster ions.[18] The production of metallofullerenes, such as those obtained by Smalley and co-workers[24] and Kroto and co-workers[26] for the case of uranium, clearly requires the use of a cluster source. In our experimental setup, LDI/LA of graphite does not yield fullerenes (easily produced via cluster sources), as can be seen in the mass spectrum presented in Figure S5 in the SI. Interestingly, the use of fullerenes as matrixes in the matrix-assisted laser desorption ionization time-of-flight mass spectrometry (MALDI/TOF-MS) analysis of uranyl nitrate did not yield any uranium fullerene or uranium carbide species.[52]

Another important aspect of the present experiments regards the use of an FTICR mass analyzer, compared with more common TOF mass analyzers coupled to LDI/LA. In the FTICR, the experimental time scale (several milliseconds) is much longer than that in a TOF instrument (several microseconds), and this has relevance for the observed species. As studied and discussed by Aubriet, Muller, and co-workers,[50,51] in the FTICR, the longer time period available after the ionization/ablation event allows for the occurrence of ion/neutral collisions, which may lead to new species by reaction or fragmentation. This suggests that the observed products of LDI/LA in an FTICR will primarily reflect the stability of the ionic species, in contrast with LDI/LA in a TOF, in which the observed species will primarily reflect their production during the LDI/LA process.

The ThC_2^+ and ThC_4^+ ions were dominant in all of the spectra, as seen in Figure 1. In Figure 2, the ThC_n^+ family was also ejected to emphasize the larger ions. Among the intriguing features apparent in Figures 1 and 2 are the high intensity of the $Th_{13}C_n^+$ cations, the low intensities of the $Th_5C_n^+$ and $Th_6C_n^+$ ions, and the relatively high intensity of the ThC_{13}^+ ion compared to ThC_7^+ to ThC_{12}^+.

A striking aspect in the case of uranium, as seen in Figure 3, is the absence of cluster species larger than $U_2C_n^+$. As in the case of thorium, UC_2^+ and UC_4^+ ions were dominant in all of the spectra and a high intensity of the UC_{13}^+ ion was also observed.

Besides the high intensities of the AnC_2^+ and AnC_4^+ ions, another common feature for both thorium and uranium in the AnC_n^+ family is the prevalence of larger species with an even number of C atoms. An enhanced stability of these species is an indication that the metal atom is connected to C_2 moieties, implying the presence of strong metal−dicarbide bonds. As indicated in the Introduction, several recent computational studies of neutral AnC_2 molecules have revealed the presence of the C_2 moiety bonded to the metal.[12−16] A computational study of ThC_4 also pointed to a C_2−Th−C_2 connectivity.[15] A theoretical study of MC_2^+ cations (M = Sc−Zn) has also evidenced the presence of C_2 units, in particular for early transition metals.[17]

The structures of the AnC_2^+ and AnC_4^+ ions were probed by CID experiments and ion/molecule reactions with oxygen. CID of AnC_2^+ showed the formation of An^+, that is, the loss of two C atoms, presumably as C_2; this is suggestive that the structures of the AnC_2^+ ions involve C_2 units, as discussed above. CID of AnC_4^+ also showed the formation of An^+, that is, the loss of C_4; in the case of thorium, formation of ThC_3^+ with elimination of carbon was also observed.

The results obtained in the reactions of AnC_2^+ and AnC_4^+ with oxygen are summarized in Table 1.

Table 1. Product Distributions, Rate Constants, and Efficiencies for Reactions of AnC_2^+ and AnC_4^+ with Oxygen

	primary product distributions	k^a	$k/k_{COL}{}^a$
ThC_2^+	Th^+ (15%), ThO^+ (45%), ThO_2^+ (25%), ThC_2O^+ (15%)	0.57	1.0
UC_2^+	U^+ (10%), UO^+ (30%), UO_2^+ (50%), UC_2O^+ (10%)	0.90	1.6
ThC_4^+	ThO^+ (90%), ThO_2^+ (10%)	0.60	1.1
UC_4^+	UO^+ (40%), UO_2^+ (60%)	0.54	1.0

[a] k and k_{COL} in units of 10^{-9} cm^3/molecule·s; the absolute values are considered accurate to ±50%; the relative values for comparative purposes are considered accurate to ±20%.

The reactions with oxygen were all very efficient, and unanticipated products were formed, AnO_2^+ in particular. Confirmation of some of the primary products was achieved by double-resonance experiments, in which a possible precursor of a secondary product, e.g., AnO^+, which could yield AnO_2^+, is continuously ejected from the FTICR cell during the reaction. In the case of thorium, it is known that ThO^+ does not lead to ThO_2^+ by reaction with oxygen.[53] Direct formation of MO_2^+ from reactions of M^+ with oxygen has been observed by Bohme and co-workers in reactions of late d transition-metal ions (Fe^+, Co^+, Ni^+, Cu^+, and Zn^+) with molecular oxygen;[54] these were slow addition reactions of oxygen that occurred with collisional stabilization of the adducts by helium in a selected ion-flow tube. Elimination of C_2 or C_4, or their combinations with oxygen, in the reactions of the AnC_2^+ and AnC_4^+ ions with oxygen is suggestive of the presence of C_2 moieties in the metal carbide ions and exchange reactions such as that given by eq 1.

$$AnC_2^+ + O_2 \rightarrow AnO_2^+ + C_2 \quad (1)$$

In contrast to slow oxygen-adduct formation, elimination of an energetic C_2 neutral enables eq 1 under low-pressure conditions in which the product is not collisionally cooled. The low-pressure conditions of the experiments ensure that only bimolecular processes occur, in this way invalidating other hypothetical processes like consecutive elimination of CO_2 and the addition of oxygen because the AnO_2^+ ions are formed as primary products.

dx.doi.org/10.1021/ic401058b | Inorg. Chem. 2013, 52, 10968−10975

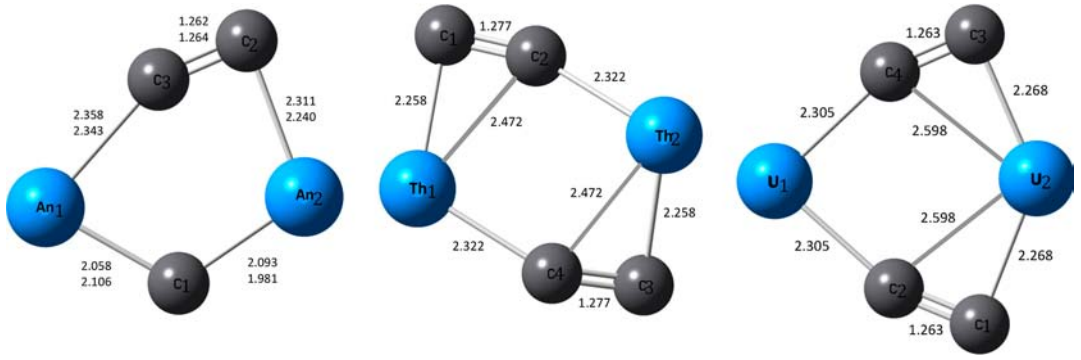

Figure 4. Computed ground-state geometries of $Th_2C_3^+$ (left, bond distances on top; doublet), $U_2C_3^+$ (left, bond distances on bottom; sextet), $Th_2C_4^+$ (middle; doublet), and $U_2C_4^+$ (right; octet). Bond distances are in angstroms. The geometries were optimized using the PBE0 functional.

The dominance of species with an even number of C atoms gives an unanticipated character to the observation of a high local intensity of the AnC_{13}^+ ions (see Figures 1 and 3). This may correspond to a change of the structures of the ions when this number of C atoms is reached, with an associated additional stability. In a theoretical study of TaC_n^+ (n = 7−13) cations,[55] which referred to experimental observations of tantalum carbide cations,[25,26] several possible isomers were examined, namely, metallacyclic, linear, bridged, atop, and metallocenic. Interestingly, metallacyclic structures, with the Ta atom incorporated into the carbon ring, were found to be the most stable for the majority of cases studied, and the carbides with an even number of C atoms appeared to exhibit enhanced stability. The evident enhanced stability of AnC_{13}^+ may suggest a similar structural phenomenon. CID and reactivity experiments were attempted with AnC_{13}^+ and other AnC_n^+ for n > 4, but the low intensity and reproducibility of the ion signals did not lead to meaningful results.

Most of the observed carbide chemistry, particularly abundance distributions, was generally quite similar for the clusters with one or two Th or U atoms (polymetallic clusters were not observed for uranium). A notable exception was the appearance of substantial $Th_2C_3^+$ versus essentially nil $U_2C_3^+$, with $U_2C_4^+$ being the smallest bimetallic uranium carbide cluster cation appearing in appreciable abundance (see Figures 1 and 3). The $An_2C_6^+$ and $An_2C_8^+$ cluster ions were similarly abundant for both thorium and uranium. The same disparity appeared using both the actinide carbide targets and the targets comprised of a mixture of the actinide oxide and graphite. Achieving the same results for very different types of solid targets points to a difference in the intrinsic stabilities of the gas-phase species rather than an artifact of the LDI synthetic process. CID experiments did not lead to meaningful results because of the low reproducibility of the ion signals; regardless, in the low-energy, multicollision conditions and long time scale of the CID experiments in the FTICR, conclusions concerning the ion stability would be rather doubtful. DFT computations of the structures and energetics of $Th_2C_3^+$, $Th_2C_4^+$, $U_2C_3^+$, and $U_2C_4^+$ were performed to elucidate the origins of the different abundance distributions.

Structures and Energetics of the $An_2C_3^+$ and $An_2C_4^+$ Clusters. The computed ground-state geometries for the four considered $An_2C_3^+$ and $An_2C_4^+$ clusters obtained at the PBE0 level are shown in Figure 4. The ground-state structures of $Th_2C_3^+$ and $U_2C_3^+$ are quite similar; the spin configurations are respectively doublet and sextet. On the other hand, the ground-state structures of $Th_2C_4^+$ (doublet spin state) and $U_2C_4^+$ (octet spin state) are different, as seen in Figure 4. In the $Th_2C_4^+$ cluster, which presents nearly planar Th−C_2−Th units, a C_2 symmetry axis perpendicular to the Th−Th orientation makes the two Th atoms equivalent. In contrast, $U_2C_4^+$ presents two nearly planar U−C_2−U units, slightly tilted with respect to one another, with a symmetry plane containing the U−U orientation and bisecting the two pairs of equivalent U−C−U planes, thus corresponding to very different coordinations of the two U atoms.

For both thorium and uranium cases, the differences in energies for the two low-lying $An_2C_4^+$ geometries were small. Specifically, for $Th_2C_4^+$, the geometry corresponding to ground-state $U_2C_4^+$ was computed to be 7.3 kJ/mol higher in energy than the ground-state $Th_2C_4^+$ geometry; for $U_2C_4^+$, the geometry corresponding to ground-state $Th_2C_4^+$ was computed to be 7.2 kJ/mol higher in energy than the ground-state $U_2C_4^+$ geometry. For the computed structures (see the SI), the spin ground states for $U_2C_n^+$ are high, namely, sextet and octet, respectively, for n = 3 and 4, whereas those for $Th_2C_n^+$ are all doublet. The structure obtained here for $U_2C_4^+$ is similar to that previously reported for neutral Y_2C_4.[56]

To evaluate the relative stabilities of the clusters, the computed atomization energies obtained at the PBE and PBE0 levels using eq 2 are given in Table 2.

$$An_2C_n^+ \rightarrow An^+ + An + nC \qquad (2)$$

Table 2. Computed Atomization Energies for $An_2C_n^+$ Clusters[a]

cluster	ΔE_{at}(PBE)	ΔE_{at}(PBE0)
$Th_2C_3^+$	28.35	27.00
$Th_2C_4^+$	34.93	33.36
$U_2C_3^+$	25.77	24.49
$U_2C_4^+$	32.44	31.33

[a] ΔE_{at} is the energy (in eV) for eq 2 for each ground-state cluster structure.

It is evident that the $Th_2C_n^+$ clusters are both more stable than the corresponding $U_2C_n^+$ clusters, by ∼2 eV (∼200 kJ/mol) or more, which appears to be independent of the choice of the functional (PBE is a "pure" DFT functional, while PBE0 includes 25% of Hartree−Fock exchange and is thus a hybrid functional). From the values in Table 2, it follows that the energies for eq 3 are nearly the same for An = Th, U: −6.58 eV (−635 kJ/mol) for Th and −6.67 eV (−644 kJ/mol) for U at

dx.doi.org/10.1021/ic401058b | Inorg. Chem. 2013, 52, 10968−10975

the PBE level and −6.37 eV (−615 kJ/mol) for Th and −6.84 eV (−660 kJ/mol) for U at the PBE0 level.

$$An_2C_3^+ + C \rightarrow An_2C_4^+ \quad (3)$$

Although the energy for eq 3 may be slightly more favorable for $U_2C_3^+$ than $Th_2C_3^+$, the very small difference is not adequate to account for the absence of $U_2C_3^+$, versus abundant $Th_2C_3^+$. A more plausible explanation for the difference between thorium and uranium is the absolute cluster stabilities, as given by the atomization energies in Table 2. The $Th_2C_3^+$ cluster is more stable toward atomization compared with $U_2C_3^+$ by some 240 kJ/mol, which could account for the appearance of $Th_2C_3^+$ and absence of $U_2C_3^+$. The $Th_2C_4^+$ cluster is also intrinsically more stable than $U_2C_4^+$, both of which are observed. The results suggest that $Th_2C_3^+$ is sufficiently stable to be produced under the experimental conditions, whereas $U_2C_3^+$ is not. This interpretation implies that an atomization energy of greater than ∼25 eV (i.e., that for $U_2C_3^+$) is necessary to appreciably produce the $An_2C_3^+$ cluster and that an energy of ∼27 eV (i.e., that for $Th_2C_3^+$) is sufficient. This interpretation, based on the stability of the potentially formed, relaxed clusters in the gas phase, is missing other factors that may thermodynamically and kinetically affect the formation of the clusters. Simulating these effects would be a highly complex task in particular because it is hard to know precisely the experimental conditions (such as the temperature) under which the (individual) clusters are formed. It is assumed that the substantial observed differences in the stabilities of the resulting clusters are governing the experimentally observed abundances. The stabilities of both of the $An_2C_4^+$ clusters are evidently adequately high to enable their formation under the experimental conditions. It should be noted that, although the ground-state structures of $Th_2C_4^+$ and $U_2C_4^+$ are different, the energy differences between the two types of low-energy structures are computed to be only a few kilojoules per mole, such that the different ground-state geometries are apparently not directly pertinent to the overall cluster stabilities and experimental observations.

ELF population analyses (see Tables S5−S8 in the SI) reveal that covalent bonding between the An and C atoms belonging to C_2 moieties is stronger than that between the An atoms and a single C atom (as can be seen in the $Th_2C_3^+$ and $U_2C_3^+$ cases), which is consistent with an exothermic reaction (eq 3). In $Th_2C_3^+$, the single C atom is strongly bound to both Th atoms (single/double bonds), while in $U_2C_3^+$, this single C atom is only chemically bound to one of the U atoms, with less electrons involved in the bond than in the previous case (corresponding essentially to a single bond). Thus, the relative instability of $U_2C_3^+$ with respect to the other considered species is mainly attributed to an inability to strongly bind the single C atom bridging the two U atoms. From the electron density population analysis (see Tables S13−S16 in the SI), one can conclude that the Th atoms adopt a +II oxidation state in both the $Th_2C_3^+$ and $Th_2C_4^+$ structures. On the other hand, in the $U_2C_3^+$ structure, one of the two U atoms also adopts a +II oxidation number, while the oxidation number of the other U atom is more ambiguous. Indeed, the presence of a bonding basin between this atom and the "lonely" C atom could be compatible with a +II or a +III oxidation number. The same ambiguity arises in the $U_2C_4^+$ structure for both U atoms, and thus we continued by performing Mulliken population analysis (see Tables 3 and 4). The Mulliken charges confirm the previous observations that, in the $An_2C_3^+$ structures, the charges on An_1 and An_2 are not equivalent although rather close to one another. In $Th_2C_4^+$, both Th atoms are equivalent by symmetry, and thus they have the same Mulliken charge, while in $U_2C_4^+$, a significant difference is observed between U_1 and U_2. In all of the structures, the C atoms have negative or zero Mulliken charges, in agreement with the electron density population analysis. Mulliken spin populations indicate that the spin density is essentially located on the An atoms. In $Th_2C_3^+$ and $Th_2C_4^+$, the unpaired electron delocalizes on both Th atoms (although it tends to localize a bit more on Th_1 in the $Th_2C_3^+$ structure). On the contrary, in $U_2C_3^+$, U_1 is credited with almost one more unpaired electron than U_2, such that the asymmetry between the two U atoms is much more significant than that between the Th atoms in $Th_2C_3^+$. Although no symmetry element relates U_1 and U_2 in $U_2C_4^+$, the Mulliken spin density population is quite similar in these two atoms.

Table 3. Mulliken Charges for $An_2C_n^+$ Clusters Obtained with the PBE0 Functional

X	An_1	An_2	C_1	C_2	C_3	C_4
$Th_2C_3^+$	0.91	0.78	−0.41	−0.27	−0.01	N/A
$Th_2C_4^+$	0.75	0.75	−0.26	0.01	−0.25	0.00
$U_2C_3^+$	1.05	0.87	−0.50	−0.28	−0.15	N/A
$U_2C_4^+$	1.11	0.74	−0.30	−0.12	−0.30	−0.12

Table 4. Mulliken Spin Population for $An_2C_n^+$ Clusters Obtained with the PBE0 Functional

X	An_1	An_2	C_1	C_2	C_3	C_4
$Th_2C_3^+$	0.58	0.40	0.00	0.06	−0.06	N/A
$Th_2C_4^+$	0.40	0.40	0.13	−0.03	0.13	−0.03
$U_2C_3^+$	3.04	2.25	−0.22	−0.02	−0.05	N/A
$U_2C_4^+$	3.64	3.41	0.13	−0.16	0.13	−0.16

CONCLUSIONS

Laser ionization of solid thorium and uranium carbide targets resulted in molecular actinide carbide clusters. Abundant AnC_2^+ and AnC_4^+ (An = Th, U) are in accordance with the stability of the C_2 moiety, with CID and reactivity with oxygen reinforcing this interpretation, which is also clearly apparent in the computed $An_2C_n^+$ cluster structures that comprise An−C_2−An units. Both UC_{13}^+ and ThC_{13}^+ exhibited anomalously high abundances, suggesting particularly stable structures; revealing the nature of these species will be a focus of future computational efforts. Several polymetallic thorium carbide clusters were observed. The appearance of unusually high abundances of $Th_{13}C_n^+$ (n = 26−30) was particularly intriguing. This result points to a particularly stable structure with 13 Th atoms; it would be very challenging to effectively model such large systems to reveal the origins of this high stability because of the size of the system and the large number of possible conformations.

A significant disparity between thorium and uranium appeared in the relative abundances of the dimer ions, $An_2C_n^+$. Whereas $Th_2C_3^+$ was substantially abundant, $U_2C_3^+$ was essentially absent, with $U_2C_4^+$ being the smallest observed uranium carbide dimer. DFT revealed that the structures of $Th_2C_3^+$ and $U_2C_3^+$ are essentially the same and that the two lowest-lying structures of the $An_2C_4^+$ clusters are close in energy for both An = Th and U. The computations revealed that the inherent stability of $Th_2C_3^+$, as indicated by its atomization energy, is greater than that of $U_2C_3^+$ by approximately 240 kJ/mol. The appearance of $Th_2C_3^+$ and

dx.doi.org/10.1021/ic401058b | Inorg. Chem. 2013, 52, 10968−10975

absence of $U_2C_3^+$ may then be attributed to this difference in stabilities.

■ ASSOCIATED CONTENT

Supporting Information

Powder X-ray diffractogram of a UC_4 sample, LDI/LA(+) mass spectra of AnC_4 without ion ejections, ThC_{11-13}^+ region of the LDI/LA(+) mass spectrum of ThC_4 in Figure 1 showing the ^{13}C isotopic peaks, LDI/LA(+) mass spectrum of a graphite sample, peak lists and ion identifications for the mass spectra in Figures 1 and 3, computed energetics and geometrical parameters for the four considered $An_2C_n^+$ cluster structures and for the isolated ions and atoms, obtained at the PBE and PBE0 levels, ELF and electron density population analyses obtained for the different species at the PBE0 level of theory. This material is available free of charge via the Internet at http://pubs.acs.org.

■ AUTHOR INFORMATION

Corresponding Authors

*E-mail: jmarcalo@ctn.ist.utl.pt.
*E-mail: gagliard@umn.edu.

Author Contributions

The manuscript was written through contributions of all authors. All authors have given approval to the final version of the manuscript.

Author Contributions

‡C.C.L.P. was the primary contributor for the experimental work.

Author Contributions

§R.M. was the primary contributor for the computational modeling.

Notes

The authors declare no competing financial interest.

■ ACKNOWLEDGMENTS

R.M. thanks David Semrouni for helpful discussions. The authors are grateful to Fundação para a Ciência e a Tecnologia/Portugal ("Ciência 2007" Programme; Ph.D. Grant SFRH/BD/70475/2010 to A.F.L.). The work by R.M., S.H. and L.G. was supported by the Director, Office of Basic Energy Sciences, U.S. Department of Energy, under Contract USDOE/DESC002183. The work by J.K.G. was fully supported by the U.S. Department of Energy, Office of Basic Energy Sciences, Heavy Element Chemistry, at LBNL under Contract DE-AC02-05CH11231.

■ REFERENCES

(1) Gupta, S. K.; Gingerich, K. A. *J. Chem. Phys.* **1980**, *72*, 2795–2800.
(2) Kohl, F. J.; Stearns, C. A. *High Temp. Sci.* **1974**, *6*, 284–302.
(3) Jackson, D. N.; Barton, G. W.; Krikorian, O. H.; Newburg, R. S. *J. Phys. Chem.* **1964**, *68*, 1516–1523.
(4) Gingerich, K. A. *Chem. Phys. Lett.* **1978**, *59*, 136–139.
(5) Sasaki, N.; Kubo, K.; Asano, M. *J. Chem. Phys.* **1973**, *59*, 4567–4568.
(6) Gupta, S.; Gingerich, K. A. *J. Chem. Phys.* **1979**, *71*, 3072–3080.
(7) Norman, J. H.; Winchell, P. *J. Phys. Chem.* **1964**, *68*, 3802–3805.
(8) Gingerich, K. A. *J. Chem. Phys.* **1969**, *50*, 2255–2256.
(9) Becker, J. S.; Dietze, H.-J. *Fresenius' J. Anal. Chem.* **1997**, *359*, 338–345.
(10) Kraiem, M.; Mayer, K.; Gouder, T.; Seibert, A.; Wiss, T.; Thiele, H.; Hiernaut, J.-P. *Int. J. Mass Spectrom.* **2010**, *289*, 108–118.
(11) Wang, X.; Andrews, L.; Malmqvist, P.-Å.; Roos, B. O.; Gonçalves, A. P.; Pereira, C. C. L.; Marçalo, J.; Godart, C.; Villeroy, B. *J. Am. Chem. Soc.* **2010**, *132*, 8484–8488.
(12) Wang, X.; Andrews, L.; Ma, D.; Gagliardi, L.; Gonçalves, A. P.; Pereira, C. C. L.; Marçalo, J.; Godart, C.; Villeroy, B. *J. Chem. Phys.* **2011**, *134*, 244313.
(13) Pogány, P.; Kovács, A.; Varga, Z.; Bickelhaupt, F. M.; Konings, R. J. M. *J. Phys. Chem. A* **2012**, *116*, 747–755.
(14) Zalazar, M. F.; Rayon, V. M.; Largo, A. *J. Phys. Chem. A* **2012**, *116*, 2972–2977.
(15) Kovács, A.; Konings, R. J. M. *J. Nucl. Mater.* **2008**, *372*, 391–393.
(16) Pogany, P.; Kovacs, A.; Szieberth, D.; Konings, R. J. M. *Struct. Chem.* **2012**, *23*, 1281–1289.
(17) Rayon, V. M.; Redondo, P.; Barrientos, C.; Largo, A. *J. Phys. Chem. A* **2007**, *111*, 6345–6353.
(18) Duncan, M. A. *Rev. Sci. Instrum.* **2012**, *83*, 041101.
(19) McIndoe, J. S. *Transition Met. Chem.* **2003**, *28*, 122–131.
(20) O'Hair, R. A. J.; Khairallah, G. N. *J. Cluster Sci.* **2004**, *15*, 331–363.
(21) Castleman, A. W., Jr. *Eur. J. Mass Spectrom.* **2007**, *13*, 7–11.
(22) Shelimov, K. B.; Clemmer, D. E.; Jarrold, M. F. *J. Chem. Soc., Dalton Trans.* **1996**, 567–574.
(23) Duncan, M. A. *J. Cluster Sci.* **1997**, *8*, 239–266.
(24) Guo, T.; Diener, M. D.; Chai, Y.; Alford, M. J.; Haufler, R. E.; McClure, S. M.; Ohno, T.; Weaver, J. H.; Scuseria, G. E.; Smalley, R. E. *Science* **1992**, *257*, 1661–1664.
(25) Infante, I.; Gagliardi, L.; Scuseria, G. E. *J. Am. Chem. Soc.* **2008**, *130*, 7459–7465.
(26) Dunk, P. W.; Kaiser, N. K.; Mulet-Gas, M.; Rodríguez-Fortea, A.; Poblet, J. M.; Shinohara, H.; Hendrickson, C. L.; Marshall, A. G.; Kroto, H. W. *J. Am. Chem. Soc.* **2012**, *134*, 9380–9389.
(27) McElvany, S. W.; Cassady, C. J. *J. Phys. Chem.* **1990**, *94*, 2057–2062.
(28) Cassady, C. J.; McElvany, S. W. *J. Am. Chem. Soc.* **1990**, *112*, 4788–4797.
(29) McElvany, S. W. *J. Phys. Chem.* **1992**, *96*, 4935–4937.
(30) Hopwood, F. G.; Fisher, K. J.; Greenhill, P.; Willett, G. D.; Zhang, R. *J. Phys. Chem. B* **1997**, *101*, 10704–10708.
(31) Zhang, R.; Achiba, Y.; Fisher, K. J.; Gadd, G. E.; Hopwood, F. G.; Ishigaki, T.; Smith, D. R.; Suzuki, S.; Willett, G. D. *J. Phys. Chem. B* **1999**, *103*, 9450–9458.
(32) Zhang, R.; Dinca, A.; Fisher, K. J.; Smith, D. R.; Willett, G. D. *J. Phys. Chem. A* **2005**, *109*, 157–164.
(33) Marçalo, J.; Santos, M.; Pires de Matos, A.; Gibson, J. K. *Inorg. Chem.* **2009**, *48*, 5055–5057.
(34) Kruger, O. L.; Armstrong, J. L. *Rev. Sci. Instrum.* **1964**, *35*, 156–158.
(35) Su, T.; Chesnavich, W. J. *J. Chem. Phys.* **1982**, *76*, 5183–5185.
(36) Lide, D. R., Ed. *CRC Handbook of Chemistry and Physics*, 88th ed.; CRC Press: Boca Raton, FL, 2007.
(37) *TURBOMOLE v6.4 2012, a development of the University of Karlsruhe and Forschungszentrum Karlsruhe GmbH, 1989–2007*; TURBOMOLE GmbH since 2007, available from http://www.turbomole.com.
(38) Schäfer, A.; Huber, C.; Ahlrichs, R. *J. Chem. Phys.* **1994**, *100*, 5829–5835.
(39) Cao, X.; Dolg, M. *J. Mol. Struct. (THEOCHEM)* **2004**, *673*, 203–209.
(40) Perdew, J. P.; Burke, K.; Ernzerhof, M. *Phys. Rev. Lett.* **1996**, *77*, 3865–3868.
(41) Perdew, J. P.; Ernzerhof, M.; Burke, K. *J. Chem. Phys.* **1996**, *119*, 9982–9985.
(42) Kovács, A.; Konings, R. J. M. *J. Phys. Chem. A* **2011**, *115*, 6646–6656.
(43) Becke, A. D.; Edgecombe, K. E. *J. Chem. Phys.* **1990**, *92*, 5397–9403.
(44) Kohout, M.; Savin, A. *Int. J. Quantum Chem.* **1996**, *60*, 875–882.
(45) Kohout, M. *DGrid*, version 4.6; 2011.

(46) Silvi, B.; Savin, A. *Nature* **1994**, *371*, 683−686.
(47) Bader, R. F. W. *Atoms in Molecules: A Quantum Theory*; Oxford University Press: New York, 1994.
(48) Amato, F.; Panyala, N. R.; Vasina, P.; Soucek, P.; Havel, J. *Rapid Commun. Mass Spectrom.* **2013**, *27*, 1196−1202.
(49) Aubriet, F.; Muller, J. F. *J. Phys. Chem. A* **2002**, *106*, 6053−6059.
(50) Aubriet, F.; Poleunis, C.; Muller, J. F.; Bertrand, P. *J. Mass Spectrom.* **2006**, *41*, 527−542.
(51) Aubriet, F.; Muller, J. F. *J. Am. Soc. Mass Spectrom.* **2008**, *19*, 488−501.
(52) Havel, J.; Soto-Guerrero, J. *J. Radioanal. Nucl. Chem.* **2005**, *263*, 489−492.
(53) Cornehl, H. H.; Wesendrup, R.; Diefenbach, M.; Schwarz, H. *Chem.—Eur. J.* **1997**, *3*, 1083−1090.
(54) Koyanagi, G. K.; Caraiman, D.; Blagojevic, V.; Bohme, D. K. *J. Phys. Chem. A* **2002**, *106*, 4581−4590.
(55) Roszak, S.; Balasubramanian, K. *Chem. Phys. Lett.* **1997**, *265*, 553−560.
(56) Roszak, S.; Balasubramanian, K. *J. Phys. Chem. A* **1998**, *102*, 6004−6009.